Injection of electron beams into two laser wakefields and generation of electron rings

Q. Chen [1], Dominika Maslarova [2,3] J. Wang [1], S. Li,[1] and D. Umstadter[1,*]

[1]*Department of Physics and Astronomy, University of Nebraska-Lincoln, Lincoln, Nebraska 68588, USA*
[2]*Institute of Plasma Physics of the Czech Academy of Sciences, Za Slovankou 1782/3, 182 00 Prague, Czech Republic*
[3]*Faculty of Nuclear Sciences and Physical Engineering, Czech Technical University in Prague,
Brehová 78/7, 115 19 Prague, Czech Republic*

Mutual injection of electron beams into two laser plasma wakefields was observed experimentally when driving laser pulses interfered in plasma at a small crossing angle and were slightly relatively delayed, approximately by one pulse duration. Particle-in-cell simulations revealed that the mutual injection was sensitive to the spatial overlap of the laser pulses, which therefore could be used to control the mutual injection. The dual synchronized, femtosecond electron beams are potentially useful for pump-probe experiments in ultrafast science. In addition, out-of-axis ring-shaped electron beams were detected in both experiments and simulations.

I. INTRODUCTION

Ultrashort, ultraintense laser pulses can drive large-amplitude plasma waves [1–4], which have been demonstrated to accelerate electron beams to the GeV level in centimeter-scale length [5,6]. These $GeV\,cm^{-1}$-level-acceleration-gradient laser plasma accelerators (LPAs) are much more compact than the conventional kilometer-scale radio-frequency accelerators, such that LPAs, as well as their secondary radiation sources, are suitable for ultrafast and high-energy density studies in university laboratories. For example, the LPA-based free electron laser, as demonstrated recently [7] (alternatively driven by particles [8]), will be a useful coherent x-ray source for probing the fundamental material behavior [9,10]. The MeV Thomson γ ray, as another example, has the potential for various nonproliferation applications [11].

Multiple synchronized, ultrashort, high-energy electron beams and their radiations are also being explored [12], because of their applications to advanced pump-probe studies of physics [13], chemistry [14], and biology [15]. Recently, an alternative method for splitting the electron beams has been demonstrated with the transient relativistic plasma grating [16], which tailors high-power laser fields, wakefield plasma waves, and electron injection. In the experiment, two almost copropagating ($10°$ crossing angle) and interfering laser pulses drive a transient relativistic electron grating [17]. The grating then channels the electrons heated by the interference into either laser wakefield for further acceleration, which is a so-called injection process [18–21]. One typical feature of this type of injection [16] is that it prefers to follow only the leading laser pulse. In the case of the perfect time overlap of the pulses, the interference causes strong density modulations in plasma grating, leading to distorted profiles of the laser pulses as well as their wakefields [22]. Due to the distorted wakefields, the injected electron beam following the leading laser could split, and its charge significantly decreases.

Based on the abovementioned plasma grating, here we present an alternative type of dual electron beam: mutual injection of electrons into dual LPAs along two different directions. It is in contrast to the previous results of multiple electron beams [12,16,23], all of which follow a single laser wakefield. The mutual injection, according to previous simulations [16], is a result of weak plasma grating driven by a nonperfect temporal overlap of laser pulses, because the weak grating barely affects the wakefields' structure and injects electrons into them. In this paper, we discuss the main characteristic of the mutual injection in more detail.

Moreover, we report observations of electron beams of half-a-ring structures. Ring electron beams accelerated by LPAs have been extensively studied in recent years. Their formation can be a consequence of several effects: splitting of an on-axis electron beam inside a cavity due to the creation of out-of-axis electron streams [24,25]; transverse density perturbations along a decreasing plasma density [26]; perpendicularly expelled, high-divergence electrons originated on the boundaries of wakefield buckets [27,28]; and the defocusing of a laser pulse induced by the generation of a wakefield [29]. In addition, the ring can be created and accelerated by Laguerre-Gaussian laser pulses [30,31]. In this work, the ring formation is triggered solely by the collision of two laser pulses, which differs from the previous studies.

The paper is structured as follows. In Sec. II, we present experimental results of mutual injection, discussing the conditions of their occurrence, the spatial shape, and the final spectrum. In Sec. III, two-dimensional (2D) and three-dimensional (3D) particle-in-cell simulations are compared with the experimental data. The summary and potential of the technique are discussed in Sec. IV.

*donald.umstadter@unl.edu
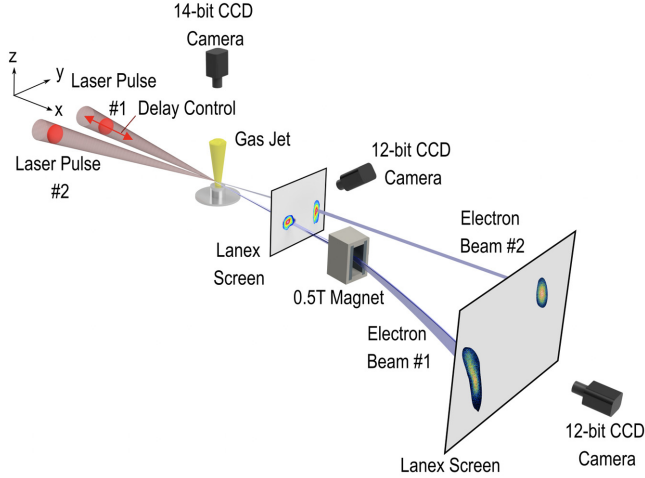
FIG. 1. Experiment schematic. Laser pulses interfere in plasma and inject electron beams into the wakefield(s). Mutual injection occurs when the two pulse's arrival time to the intersection point differ by about one pulse duration. The delay was controlled by a delay line for the collimated beam in the upstream of the off-axis parabolic mirror.

II. EXPERIMENTAL RESULTS

A. Experimental setup

The experiment was conducted at the Extreme Light Laboratory at the University of Nebraska-Lincoln, using the Diocles Ti:sapphire laser. In the single-pulse mode, the Diocles laser has a central wavelength of 800 nm, a pulse duration of $\tau_0 = 35$ fs at the full width half maximum (FWHM) of its intensity, and a peak power up to 40 TW. In the dual-pulse mode, after stretching and amplification, the laser pulse was split into two similar, copropagating pulses using a nearly $R50/T50$ beam splitter. The two pulses were then compressed to FWHM pulse durations of $\tau_1 = 39$ fs and $\tau_2 = 35$ fs, respectively. Each laser pulse was then focused by an $f/14$ off-axis parabola system to a FWHM spot size of $\omega_0 = 18\,\mu$m and into a 2-mm round gas jet, as shown in Fig. 1. The peak normalized laser vector potentials in vacuum were estimated to be $a_{0,1} \sim 1.37$ and $a_{0,2} \sim 1.52$, respectively. The angle of laser intersection was fixed at $\theta = 10°$ due to restriction of the experimental setup, while the relative delay τ_d between the two pulses on arriving to the intersection point was controllable using a motorized linear stage between the amplifier and the compressor, with minimum step size of 0.1 μm ($\sim$7 fs accuracy). A gas mixture of 99% He and 1% N_2 was used during the experiment, and its density was controlled by changing the backpressure of the ultrasonic gas jet. The spatial profiles of the electron beams were recorded using a fluorescent screen (fast lanex) paired with a 12-bit CCD camera. The electron beam energy spectrum was measured using a magnetic spectrometer with a 0.5-T, 5-cm-long dipole magnet and a second Lanex screen imaged by another 12-bit CCD camera.

B. Observation of mutual injection

To achieve a high-quality wakefield driven by only one laser pulse (such as laser pulse #1 in Fig. 1), both the laser pulse and the plasma target need to be optimized. For instance,
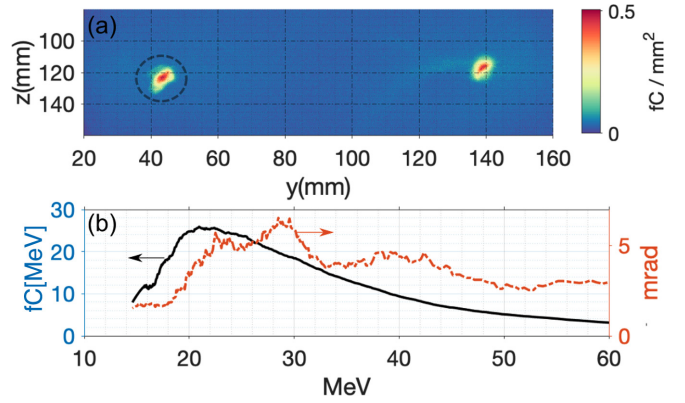
FIG. 2. Experimentally observed mutual injection electron beams. (a) Typical spatial profiles. (b) The spectrum (black solid curve) and the angular divergence (red dotted curve) for the circled left beam in panel (a).

the laser intensity and the plasma density should be low enough to suppress (self-)injection, meanwhile high enough to sustain a high-acceleration gradient. Moreover, a mixture of 99% helium and 1% nitrogen, other than pure helium, was used for a much easier injection just above the threshold density, to ensure a more stable, higher-quality wakefield for optical injection. Last, the position of the gas jet was adjusted, particularly longitudinally, with respect to the laser focus, so that the propagation of the laser pulse and its wakefield could be stabilized.

Just below the threshold density near $n_e \approx 5 \times 10^{18}\,\mathrm{cm}^{-3}$, at which injection of any kind by a single laser pulse was fully suppressed, another intense laser pulse (laser pulse #2 in Fig. 1) was added to spatiotemporally overlap with the wakefield driving laser pulse (laser pulse #1 in Fig. 1). After accurately adjusting the temporal overlap of the two pulses, from $-2\tau_0$ to $2\tau_0$ (70 fs), optical injections could be enabled and tuned. While the majority of shots demonstrated injection into one of the wakefields driven by either of the two laser pulses [16], mutual injection into both wakefields was observed at a delay of $\sim\tau_0$. Figure 2(a) shows the spatial profiles of the mutually injected electron beams on the first Lanex screen. These electron beams typically have a charge of hundreds of femtocoulombs and a quasimonoenergetic spectrum that peaks around 20 MeV, as shown in Fig. 2(b).

Besides the case of mutual injection shown in Fig. 2, more patterns of dual beams in two respective directions were observed for the same laser plasma parameters, such as those shown in Fig. 3. The electron beam following pulse #1 can further split into two beams [Figs. 3(b) and 3(c)] and three beams [Fig. 3(d)]. This is similar to the previous results of multidimensional splitting of the electron beams along one laser pulse [16], and both could be due to the spatial mismatch of two laser pulses. More specifically, although the mutual injection occurred when the delay between laser pulses was fixed around $\sim\tau_0$, the respective pointing for beams still fluctuated at 20 μrad, or equivalently one beam size level. This relative large pointing fluctuation could have caused the pulses to be mismatched in the z direction, such that the interference became multidimensional (off-axis). The effect of the direct
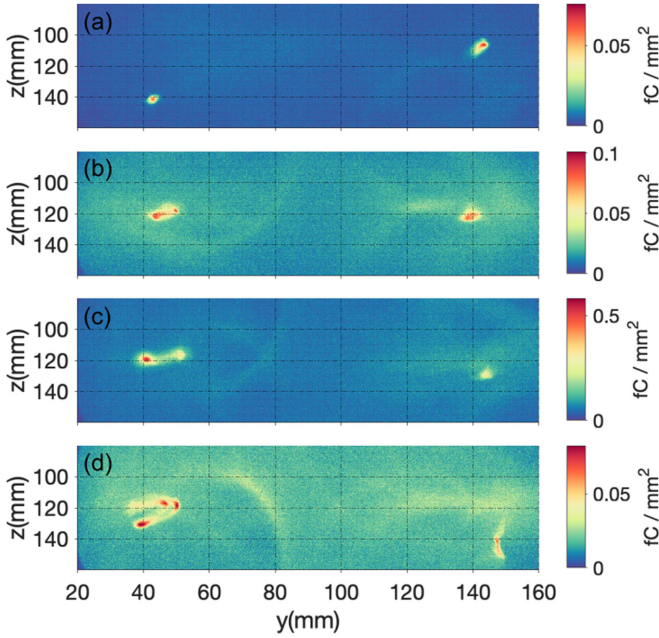
FIG. 3. Shot-to-shot varying electron beam profiles in the mutual injection experiment. Various forms of dual electron beams could have been caused by the unstable interference and injection due to the pointing jitter of laser pulses. The right-hand side beam followed the ahead laser pulse #1, and the left-hand side beam followed the delayed laser pulse #2. The ring electrons appeared more on the pulse #2 side, similar to simulations results, as shown in Fig. 5.

influence of the off-axis position of the injection pulse on the electron beam dynamics has been reported previously [32]. In our case, the interference deviated from matched (on-axis) cases and affected the shape of the electron beams accordingly, as shown by the simulation results in the next section.

III. SIMULATION RESULTS

A. Particle-in-cell simulation setup

In order to verify basic features of mutual injection, 2D and 3D particle-in-cell simulations were performed in the SMILEI code [33]. The laser pulses had parameters similar to those in the experiment: $a_{0,1} = 1.52$, $a_{0,2} = 1.37$, and $\tau_{0,1} = \tau_{0,2} = 29$ fs. In the simulations, mutual injection was observed for values from $\Delta t = 1.2\tau$ to $\Delta t = 2.2\tau$ (see the Appendix). The simulations in this section were performed for $\Delta t = 2\tau$, in order to demonstrate the basic features of the mechanism.

The pulses were moving in the x-y plane, along the positive x direction, under the angles $\alpha_1 = \theta/2 = 5°$ (pulse ahead) and $\alpha_2 = -\theta/2 = 5°$ (delayed pulse) from the x axis. Both were linearly polarized in the x-y plane. The pulse waist at the focus was $w_0 = 14$ μm, corresponding to the vacuum Rayleigh length $\pi w_0^2/\lambda = 0.77$ mm, where $\lambda = 800$ nm is the laser wavelength.

According to our previous investigation, the ionization effects do not play a notable role in the optical injection process; thus, conditions of preionized plasma were simulated by using only electron macroparticles in the simulation windows.

The 2D simulation box had a size of $L_x \times L_y = 624 \times 224$ μm^2, starting with a 50-μm linear density up-ramp,
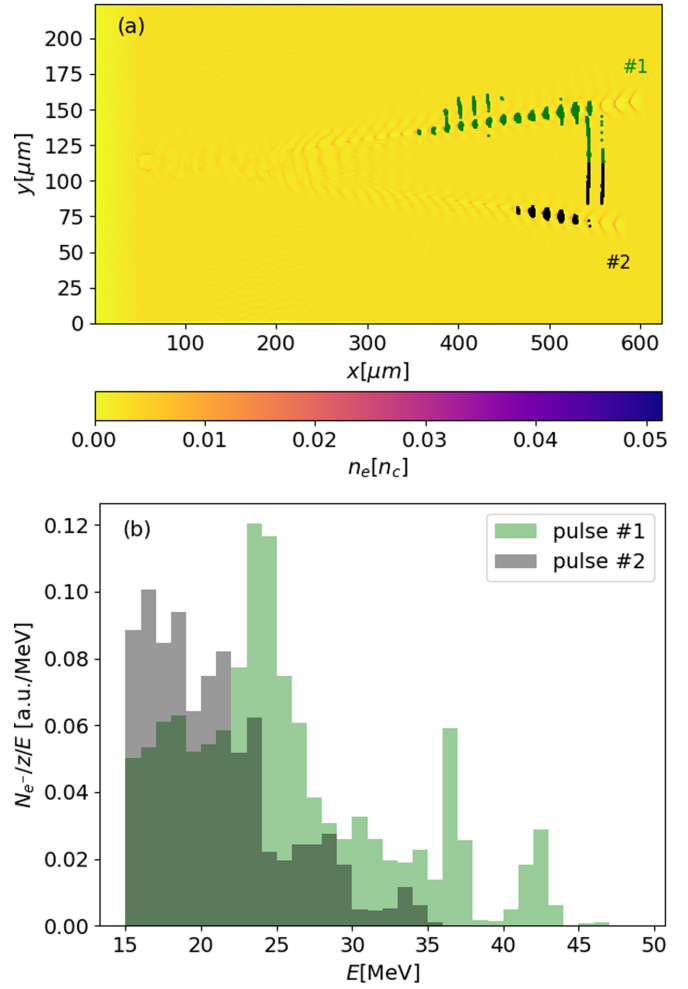
FIG. 4. 2D simulation results. (a) Electron density profile at the simulation time of $t = 2.17$ ps. The green and black dots correspond to the positions of electrons of energy higher than 15 MeV, in the direction of pulse #1 ($y > L_y/2$, wakefield ahead) and the direction of pulse #2 ($y < L_y/2$, delayed wakefield), respectively. (b) Corresponding energy spectrum of the electrons of >15 MeV from panel (a), corresponding to the direction of pulse #1 (green) and to the direction of pulse #2 (black). The overlap portions of the histograms are colored in dark green.

followed by a subsequent electron density plateau of $n_e = 5 \times 10^{18}$ cm^{-3}. Each cell had a size of $\Delta x \times \Delta y = 0.033 \times 0.067$ μm^2 and contained four electron macroparticles. The pulses were focused at $(x_f, y_f) = (100 \ \mu$m$, L_y/2)$.

The 3D simulation box had a size of $L_x \times L_y \times L_z = 358.4 \times 120 \times 64$ μm^3, starting with a 5-μm-long vacuum entrance and followed by a 10-μm linear density up-ramp and a subsequent electron density plateau of $n_e = 5 \times 10^{18}$ cm^{-3}. Each cell had a size of $\Delta x \times \Delta y \times \Delta z = 0.044 \times 0.133 \times 0.533$ μm^3 and contained two electron macroparticles. The pulses were focused at $(x_f, y_f, z_f) = (20 \ \mu$m$, L_y/2, L_z/2)$.

B. Spectrum of the electron beams

First, we demonstrate typical characteristic electron spectra in the mutual injection via 2D simulations. Figure 4 depicts the electron plasma density profile [panel (a)] and the

corresponding energy spectrum of accelerated electrons of >15 MeV [panel (b)] at the final time of the simulation, when pulses propagated around half a millimeter behind their former overlap at the focus. At this time, the pulses and first buckets of the wakefields were well separated; therefore, it was possible to observe formation of compact beams from the electrons that had become trapped in the wakefields.

Most of the energetic electrons were spread through several wakefield buckets. The first bucket with trapping was the fourth one behind pulse #1 and the third one behind pulse #2. This indicates that the first electrons in the train were temporally separated by $\Delta t_{e^-} = \Delta t - \lambda_p/c$, where λ_p is the plasma wavelength, which corresponds to $\Delta t_{e^-} = -20.5$ fs for the choice of parameters in the simulation.

Note that some electrons of high energy are also present in the area between the two wakefields. These electrons were preaccelerated during the time when the two laser pulses were significantly overlapping and, consequently, created a compound wakefield. After the two pulses propagated away from each other and generated completely separated wakefields, these stripes of electrons were not expected to gain energy and stay collimated anymore. Similar patterns of electron tails prolonged towards the middle area between the two electron beams, in the direction parallel to the y axis, were also observed in the experiment [see Figs. 2(a) and 3].

In the beam spectra shown in Fig. 4, the formation of the peaks in the spectra starts to be observable in $E_{\text{peak}_1} = 25$ MeV and $E_{\text{peak}_2} = 16$ MeV for beam #1 and beam #2,
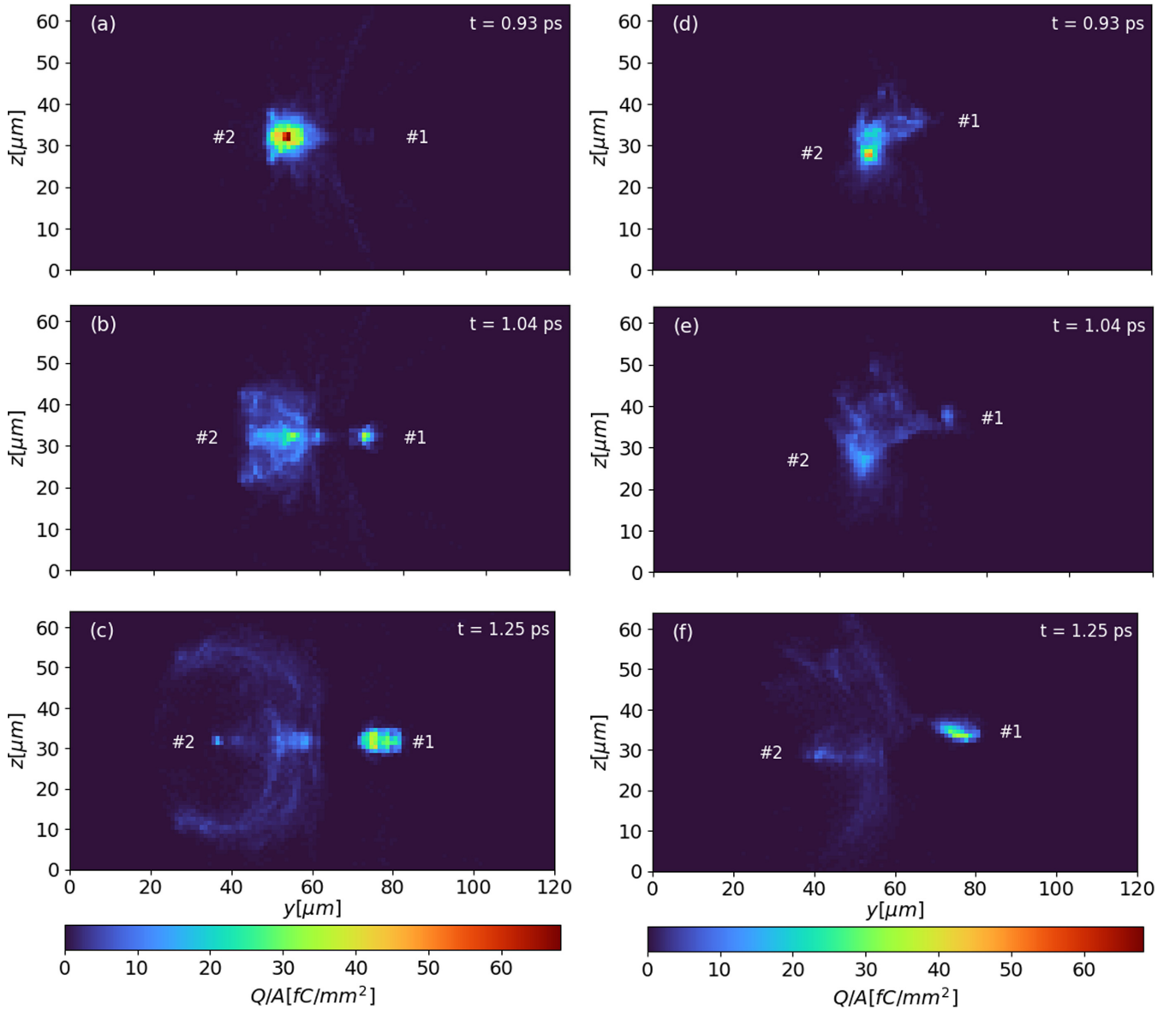
FIG. 5. Front view (charge over area Q/A) of electron beams from the 3D simulations depicting electrons of $E \geqslant 5$ MeV, with $\Delta z_{\text{foci}} = 0$ at the simulation times of (a) $t = 0.93$ ps, (b) $t = 1.04$ ps, and (c) $t = 1.25$ ps; and with $\Delta z_{\text{foci}} = 8\ \mu$m at the simulation times of (d) $t = 0.93$ ps, (e) $t = 1.04$ ps, and (f) $t = 1.25$ ps. The laser beam ahead, #1, is moving in the direction of increasing y, and the delayed beam, #2, is moving in the direction of decreasing y, as indicated by the labels in the figures. The time of the focus collision corresponds to the simulation time of $t = 0.12$ ps. The center of the collision is located in the plane $y = 60\ \mu$m.

respectively. In simulations, we also observed local maxima at the tail of the spectrum coming from electrons at the front beams that experienced higher accelerating field. This was not captured by experimental diagnostics presumably due to the lower spectrometer resolution.

C. Transversely mismatched mutual beams and electron ring formation

Due to the computationally demanding simulation geometry, we performed 3D simulations for the initial stages of the injection process only. Two simulations were carried out, one without a misalignment of laser foci in the z direction, $\Delta z_{\text{foci}} = 0 \ \mu\text{m}$, and the other with a misalignment of $\Delta z_{\text{foci}} = 8 \ \mu\text{m}$ (the centers of the laser pulses were shifted in the z direction by $+4 \ \mu\text{m}$ and -4 for pulse #1 and pulse #2, respectively).

The profiles of the electron beams in the y-z plane show the main characteristics of the propagation of energetic electrons in the transverse directions (see Fig. 5). Without misalignment for laser foci in the z direction, the centers of the electron beams are aligned as well [see Fig. 5(c)]. There is also a significant amount of energetic electrons between and around the area of the two electron beams, as predicted by the experiment and 2D simulations [see Figs. 4(a) and 3].

These electrons gained energy during the collision. They were originally traveling from the central part of the collision towards the direction of the wakefield of the delayed pulse #2, in the same manner as the main electron beam trapped on the axis [Fig. 5(a)]. However, they were not trapped in the wakefield, but became separated from the main beam and escaped radially outward [Fig. 5(b)]. Resultantly, an annular structure around the bucket boundaries was formed Fig. 5(c)]. This is similar to previous studies, where preaccelerated untrapped electrons traversed behind the bubble but did not enter the wakefield, forming an electron ring [27,28]. However, in the case of optical injection discussed in this work, the electrons are expelled dominantly towards the center of collision, forming a half-a-ring beam rather than the full structure. This is a consequence of heating the electrons only in the central area between the wakefields, which led to the radial asymmetry.

The formation of the electron beams is similar for the case with a misalignment, as depicted in Figs. 5(d) and 5(f). However, the beam profiles, especially the one of beam #1, are tilted. This confirms that fluctuation in the pointing jitter in the experiment can lead to significant deviations of the beam profiles from shot to shot. In addition, the ring patterns are affected as well [see Fig. 5(c) vs Fig. 5(f)].

IV. SUMMARY AND DISCUSSION

In conclusion, we have demonstrated mutual injection into two laser wakefields. The injection was triggered by two, almost identical, laser pulses colliding at a $10°$ angle in underdense plasmas. The occurrence of two electron beams in the experiment was dependent on a temporal delay between the two pulses. Particle-in-cell simulations reproduced the presence of mutual injection and revealed that electrons were injected into multiple wakefield buckets, forming two trains of short electron beams delayed by a few tens of femtoseconds.

This property can be utilized, for instance, in femtosecond radioanalysis [34,35].

In order to introduce the technique for the practical applications, it will be necessary to achieve higher reproducibility of the mutual injection in future experiments and more detailed examination on parameters such as the laser focus position and the collision angle will be required. Moreover, partial ring electron beams were formed out of the wakefield area. The ring formation was a consequence of the pulse collision, which differs from other observations of the ring electron beams reported previously [24–28].

Possible reasons for the rare occurrence of the mutual injection at $|\Delta t| \sim 1\tau$ in the experiment compared to a wider delay range of $|\Delta t| \sim 1.2\tau$–2.2τ in the simulations could be caused by several combined factors. For example, the laser pointing jitter of $\sim 1\tau$ in the experiment could have aggregated the actual overall spatiotemporal mismatch from $\sim 1\tau$ to $\sim 2\tau$, more similar to simulation results. Such a transverse misalignment in the z direction could also significantly change the electron beam shape, as indicated in Sec. II B of this work. In addition, the laser parameters in the experiment were measured and optimized at much attenuated intensity, while those parameters for the full-power laser pulses were unknown and should be characterized by some high-power-mode imager [36]. Those measurements could also indicate the quality of spatial overlap and provide more accurate parameters for simulations.
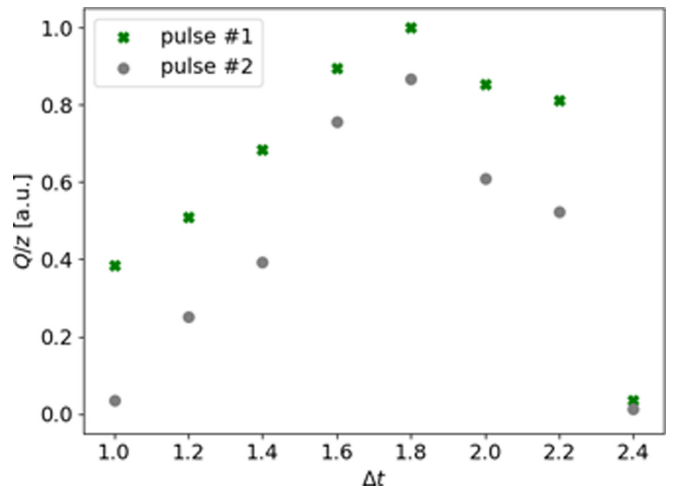
FIG. 6. 2D simulation results: Dependence of charge of electrons of energy higher than 15 MeV Q/z on Δt, at the simulation time of $t = 2.17$ ps. The green crosses and grey dots correspond to the charge in the direction of the pulse #1 ($y > L_y/2$, wakefield ahead) and the direction of the pulse #2 ($y < L_y/2$, delayed wakefield), respectively. The charge is expressed as charge per length z, since 2D data are presented. The values are normalized to the highest value in the plot (at $\Delta t = 1.8\tau$).

APPENDIX

Here, we show how the delay between the two pulses Δt changes the charge of injected electron beams. The result confirms our previous work [16], where similar laser-plasma parameters were simulated, and mutual injection was observed for $\Delta t = 1.5\tau$ and $\Delta t = 2\tau$. For $\Delta t = 0.5\tau$ and $\Delta t = 1\tau$, the interference deteriorated the quality of the delayed wakefield, and only injection in the wakefield ahead was observed. For $\Delta t = 2.5\tau$, the small-scale overlap was inefficient to trigger the optical injection.

In Fig. 6, a finer sampling in the range from $\Delta t = 1\tau$ to $\Delta t = 2.4\tau$ is presented. The simulation parameters were the same as described in Sec. III A, only the delay between the pulses Δt was accordingly changed. As expected, for $\Delta t = 1\tau$, injection into the wakefield ahead was observed only. For $\Delta t = 1.2\tau$, 1.4τ, 1.6τ, and 1.8τ, mutual injection was detected, and the charge was gradually increasing within this range, peaking at $\Delta t = 1.8\tau$. Subsequently, the charge slightly decreased for $\Delta t = 2\tau$, $\Delta t = 2.2\tau$, while mutual injection was still clearly present. For $\Delta t = 2.4\tau$, injections into both wakefields were negligible.

[1] T. Tajima and J. M. Dawson, Laser Electron Accelerator, Phys. Rev. Lett. **43**, 267 (1979).

[2] P. Sprangle, G. Joyce, E. Esarey, and A. Ting, Laser wakefield acceleration and relativstic optical guiding, in *AIP Conference Proceedings* (American Institute of Physics, College Park, MD, 1988), Vol. 175, pp. 231–239.

[3] A. Modena, Z. Najmudin, A. Dangor, C. Clayton, K. Marsh, C. Joshi, V. Malka, C. Darrow, C. Danson, D. Neely *et al.*, Electron acceleration from the breaking of relativistic plasma waves, Nature (London) **377**, 606 (1995).

[4] D. Umstadter, S.-Y. Chen, A. Maksimchuk, G. Mourou, and R. Wagner, Nonlinear optics in relativistic plasmas and laser wake field acceleration of electrons, Science **273**, 472 (1996).

[5] W. P. Leemans, B. Nagler, A. J. Gonsalves, C. Tóth, K. Nakamura, C. G. Geddes, E. Esarey, C. Schroeder, and S. Hooker, GeV electron beams from a centimetre-scale accelerator, Nat. Phys. **2**, 696 (2006).

[6] A. J. Gonsalves, K. Nakamura, J. Daniels, C. Benedetti, C. Pieronek, T. C. H. de Raadt, S. Steinke, J. H. Bin, S. S. Bulanov, J. van Tilborg, C. G. R. Geddes, C. B. Schroeder, C. Tóth, E. Esarey, K. Swanson, L. Fan-Chiang, G. Bagdasarov, N. Bobrova, V. Gasilov, G. Korn *et al.*, Petawatt Laser Guiding and Electron Beam Acceleration to 8 GeV in a Laser-Heated Capillary Discharge Waveguide, Phys. Rev. Lett. **122**, 084801 (2019).

[7] W. Wang, K. Feng, L. Ke, C. Yu, Y. Xu, R. Qi, Y. Chen, Z. Qin, Z. Zhang, M. Fang *et al.*, Free-electron lasing at 27 nanometres based on a laser wakefield accelerator, Nature (London) **595**, 516 (2021).

[8] R. Pompili, D. Alesini, M. Anania, S. Arjmand, M. Behtouei, M. Bellaveglia, A. Biagioni, B. Buonomo, F. Cardelli, M. Carpanese *et al.*, Free-electron lasing with compact beam-driven plasma wakefield accelerator, Nature (London) **605**, 659 (2022).

[9] S. Corde, K. Ta Phuoc, G. Lambert, R. Fitour, V. Malka, A. Rousse, A. Beck, and E. Lefebvre, Femtosecond x rays from laser-plasma accelerators, Rev. Mod. Phys. **85**, 1 (2013).

[10] C. Bostedt, S. Boutet, D. M. Fritz, Z. Huang, H. J. Lee, H. T. Lemke, A. Robert, W. F. Schlotter, J. J. Turner, and G. J.

Williams, Linac coherent light source: The first five years, Rev. Mod. Phys. **88**, 015007 (2016).

[11] C. Geddes, B. Ludewigt, J. Valentine, B. Quiter, M.-A. Descalle, G. Warren, M. Kinlaw, S. Thompson, D. Chichester, C. Miller *et al.*, Impact of monoenergetic photon sources on nonproliferation applications, Techical Report (Idaho National Laboratory, Idaho Falls, ID, 2017), https://www.osti.gov/biblio/1376659/.

[12] J. Wenz, A. Döpp, K. Khrennikov, S. Schindler, M. Gilljohann, H. Ding, J. Götzfried, A. Buck, J. Xu, M. Heigoldt *et al.*, Dual-energy electron beams from a compact laser-driven accelerator, Nat. Photonics **13**, 263 (2019).

[13] J. Ullrich, A. Rudenko, and R. Moshammer, Free-electron lasers: New avenues in molecular physics and photochemistry, Annu. Rev. Phys. Chem. **63**, 635 (2012).

[14] A. H. Zewail, Femtochemistry: Atomic-scale dynamics of the chemical bond, J. Phys. Chem. A **104**, 5660 (2000).

[15] V. Sundström, Femtobiology, Annu. Rev. Phys. Chem. **59**, 53 (2008).

[16] Q. Chen, D. Maslarova, J. Wang, S. X. Lee, V. Horný, and D. Umstadter, Transient Relativistic Plasma Grating to Tailor High-Power Laser Fields, Wakefield Plasma Waves, and Electron Injection, Phys. Rev. Lett. **128**, 164801 (2022).

[17] D. Mašlárová, V. Horný, Q. Chen, J. Wang, S. Li, and D. Umstadter, Generation of a static plasma electron grating, Proc. SPIE Int. Soc. Opt. Eng. **11779**, 1177907 (2021).

[18] D. Umstadter, J. K. Kim, and E. Dodd, Laser Injection of Ultrashort Electron Pulses into Wakefield Plasma Waves, Phys. Rev. Lett. **76**, 2073 (1996).

[19] E. Esarey, R. F. Hubbard, W. P. Leemans, A. Ting, and P. Sprangle, Electron Injection into Plasma Wakefields by Colliding Laser Pulses, Phys. Rev. Lett. **79**, 2682 (1997).

[20] J. Faure, C. Rechatin, A. Norlin, A. Lifshitz, Y. Glinec, and V. Malka, Controlled injection and acceleration of electrons in plasma wakefields by colliding laser pulses, Nature (London) **444**, 737 (2006).

[21] J. Faure, C. Rechatin, A. Norlin, F. Burgy, A. Tafzi, J.-P. Rousseau, and V. Malka, Controlled electron injection in a

laser-plasma accelerator, Plasma Phys. Controlled Fusion **49**, B395 (2007).

[22] V. Malka, J. Faure, C. Rechatin, A. Ben-Ismaïl, J. Lim, X. Davoine, and E. Lefebvre, Laser-driven accelerators by colliding pulses injection: A review of simulation and experimental results, Phys. Plasmas **16**, 056703 (2009).

[23] G. Golovin, W. Yan, J. Luo, C. Fruhling, D. Haden, B. Zhao, C. Liu, M. Chen, S. Chen, P. Zhang, S. Banerjee, and D. Umstadter, Electron Trapping from Interactions between Laser-Driven Relativistic Plasma Waves, Phys. Rev. Lett. **121**, 104801 (2018).

[24] B. B. Pollock, F. S. Tsung, F. Albert, J. L. Shaw, C. E. Clayton, A. Davidson, N. Lemos, K. A. Marsh, A. Pak, J. E. Ralph, W. B. Mori, and C. Joshi, Formation of Ultrarelativistic Electron Rings from a Laser-Wakefield Accelerator, Phys. Rev. Lett. **115**, 055004 (2015).

[25] A. Maitrallain, E. Brunetti, M. Streeter, B. Kettle, R. Spesyvtsev, G. Vieux, M. Shahzad, B. Ersfeld, S. Yoffe, A. Kornaszewski *et al.*, Parametric study of high-energy ring-shaped electron beams from a laser wakefield accelerator, New J. Phys. **24**, 013017 (2022).

[26] T. Z. Zhao, K. Behm, C. F. Dong, X. Davoine, S. Y. Kalmykov, V. Petrov, V. Chvykov, P. Cummings, B. Hou, A. Maksimchuk, J. A. Nees, V. Yanovsky, A. G. R. Thomas, and K. Krushelnick, High-Flux Femtosecond X-Ray Emission from Controlled Generation of Annular Electron Beams in a Laser Wakefield Accelerator, Phys. Rev. Lett. **117**, 094801 (2016).

[27] X. Yang, E. Brunetti, D. R. Gil, G. Welsh, F. Li, S. Cipiccia, B. Ersfeld, D. Grant, P. Grant, M. Islam *et al.*, Three electron beams from a laser-plasma wakefield accelerator and the energy apportioning question, Sci. Rep. **7**, 1 (2017).

[28] K. Behm, A. Hussein, T. Zhao, S. Dann, B. Hou, V. Yanovsky, J. Nees, A. Maksimchuk, W. Schumaker, A. Thomas *et al.*, Measurements of electron beam ring structures from laser

wakefield accelerators, Plasma Phys. Controlled Fusion **61**, 065012 (2019).

[29] P. Valenta, G. Grittani, C. Lazzarini, O. Klimo, and S. Bulanov, On the electromagnetic-electron rings originating from the interaction of high-power short-pulse laser and underdense plasma, Phys. Plasmas **28**, 122104 (2021).

[30] J. Vieira and J. T. Mendonça, Nonlinear Laser Driven Donut Wakefields for Positron and Electron Acceleration, Phys. Rev. Lett. **112**, 215001 (2014).

[31] G.-B. Zhang, M. Chen, C. Schroeder, J. Luo, M. Zeng, F.-Y. Li, L.-L. Yu, S.-M. Weng, Y.-Y. Ma, T.-P. Yu *et al.*, Acceleration and evolution of a hollow electron beam in wakefields driven by a Laguerre-Gaussian laser pulse, Phys. Plasmas **23**, 033114 (2016).

[32] G. Zhang, M. Chen, X. Yang, F. Liu, S. Weng, Y. Ma, D. Zou, T. Yu, F. Shao, and Z. Sheng, Betatron radiation polarization control by using an off-axis ionization injection in a laser wakefield acceleration, Opt. Express **28**, 29927 (2020).

[33] J. Derouillat, A. Beck, F. Pérez, T. Vinci, M. Chiaramello, A. Grassi, M. Flé, G. Bouchard, I. Plotnikov, N. Aunai *et al.*, SMILEI: A collaborative, open-source, multi-purpose particle-in-cell code for plasma simulation, Comput. Phys. Commun. **222**, 351 (2018).

[34] J. Yang, T. Kondoh, A. Yoshida, and Y. Yoshida, Double-decker femtosecond electron beam accelerator for pulse radiolysis, Rev. Sci. Instrum. **77**, 043302 (2006).

[35] K. Kan, T. Kondoh, J. Yang, A. Ogata, K. Norizawa, and Y. Yoshida, Development of double-decker pulse radiolysis, Rev. Sci. Instrum. **83**, 073302 (2012).

[36] A. Jeandet, A. Borot, K. Nakamura, S. W. Jolly, A. J. Gonsalves, C. Tóth, H.-S. Mao, W. P. Leemans, and F. Quéré, Spatio-temporal structure of a petawatt femtosecond laser beam, J. Phys. Photonics **1**, 035001 (2019).